

Dynamical Packing in the Habitable Zone: The Case of Beta CVn

STEPHEN R. KANE,¹ MARGARET C. TURNBULL,² BENJAMIN J. FULTON,³ LEE J. ROSENTHAL,⁴ ANDREW W. HOWARD,⁴
HOWARD ISAACSON,^{5,6} GEOFFREY W. MARCY,⁵ AND LAUREN M. WEISS⁷

¹*Department of Earth and Planetary Sciences, University of California, Riverside, CA 92521, USA*

²*SETI Institute, Carl Sagan Center for the Study of Life in the Universe, Off-Site: 2613 Waunona Way, Madison, WI 53713, USA*

³*Caltech/IPAC-NASA Exoplanet Science Institute, Pasadena, CA 91125, USA*

⁴*Department of Astronomy, California Institute of Technology, Pasadena, CA 91125, USA*

⁵*Department of Astronomy, University of California, Berkeley, CA 94720, USA*

⁶*Centre for Astrophysics, University of Southern Queensland, Toowoomba, QLD 4350, Australia*

⁷*Institute for Astronomy, University of Hawai'i, Honolulu, HI 96822, USA*

ABSTRACT

Uncovering the occurrence rate of terrestrial planets within the Habitable Zone (HZ) of their host stars has been a particular focus of exoplanetary science in recent years. The statistics of these occurrence rates have largely been derived from transiting planet discoveries, and have uncovered numerous HZ planets in compact systems around M dwarf host stars. Here we explore the width of the HZ as a function of spectral type, and the dynamical constraints on the number of stable orbits within the HZ for a given star. We show that, although the Hill radius for a given planetary mass increases with larger semi-major axis, the width of the HZ for earlier-type stars allows for more terrestrial planets in the HZ than late-type stars. In general, dynamical constraints allow ~ 6 HZ Earth-mass planets for stellar masses $\gtrsim 0.7M_{\odot}$, depending on the presence of farther out giant planets. As an example, we consider the case of Beta CVn, a nearby bright solar-type star. We present 20 years of radial velocities (RV) from the Keck/HIRES and APF instruments and conduct an injection-recovery analysis of planetary signatures in the data. Our analysis of these RV data rule out planets more massive than Saturn within 10 AU of the star. These system properties are used to calculate the potential dynamical packing of terrestrial planets in the HZ and show that such nearby stellar targets could be particularly lucrative for HZ planet detection by direct imaging exoplanet missions.

Keywords: astrobiology – planetary systems – planets and satellites: dynamical evolution and stability
– stars: individual (Beta CVn)

1. INTRODUCTION

The common exoplanet detection techniques of transits and radial velocities (RV) both have a bias towards short-period orbits (Kane & von Braun 2008). The advantage of this bias is that it has enabled a thorough exploration of multiple planet systems that exists in closely spaced orbits, often in extreme insolation flux environments, referred to as “compact systems”. The architecture and dynamics of compact planetary systems have been previously studied in detail (Ford 2014), including the dynamical connection to formation (Kane et al. 2013; Pu & Wu 2015) and the exclusion of moons (Kane 2017). Barnes & Quinn (2004) suggested

that planetary systems may have quantifiable limits to the dynamically allowed number of planets. Simulations by Smith & Lissauer (2009, 2010) and Obertas et al. (2017) investigated dynamical interactions within compact systems for the specific solar case and found a dependence on planet mass and initial spacing. A statistical analysis of compact systems by Fang & Margot (2013) indicated that compact systems are dynamically “packed”, with few dynamically viable options for additional planets in these systems. Furthermore, the presence of farther planetary companions in compact systems can be effectively constrained due to their disrupting influence on the inner planets (Becker & Adams 2017).

Of particular interest are those planets that lie within the Habitable Zone (HZ) of their host stars, where

liquid water may be present on the planetary surface given sufficient atmospheric pressure (Kasting et al. 1993; Kopparapu et al. 2013, 2014). Dynamics of planetary systems have been used to determine orbital effects in the HZ (Kane 2015; Agnew et al. 2019), as well as potentially predicting additional HZ planets (Kopparapu et al. 2009; Kopparapu & Barnes 2010). Several compact planetary systems have been discovered that harbor more than one planet in the HZ, including GJ 667C (Anglada-Escudé et al. 2013), TRAPPIST-1 (Gillon et al. 2017; Luger et al. 2017), and Teegarden’s star (Zechmeister et al. 2019). Compact HZ systems around M dwarfs may benefit from numerous architectural biases for low-mass stars. For example, it has been suggested from observational data that giant planets are relatively rare around M dwarfs (Endl et al. 2006; Cumming et al. 2008; Johnson et al. 2010; Bonfils et al. 2013) and that this may influence the habitability of terrestrial planets in those systems (Horner & Jones 2008; Shields et al. 2016; Kane & Blunt 2019). The inventory of confirmed exoplanets provided by the NASA Exoplanet Archive (Akeson et al. 2013), extracted 2020 May 11, indicates that planets more massive than 0.5 Jupiter masses orbiting stars less massive than 0.5 solar masses comprise less than 2% of the total RV exoplanet discoveries. The architecture, exoplanet detection sensitivity, and prevalence of HZ planets in M dwarf systems clearly play significant roles in calculations of occurrence rates of HZ terrestrial planets (Catanzarite & Shao 2011; Dressing & Charbonneau 2013; Gaidos 2013; Kopparapu 2013; Foreman-Mackey et al. 2014; Dressing & Charbonneau 2015). The dynamics and prevalence of HZ terrestrial planets have yet to be as rigorously tested around solar-type stars.

A star of particular interest is the nearby (8.44 pcs) star Beta Canum Venaticorum. Being a naked eye star ($V = 4.26$), the star has various designations (HD 109358, HIP 61317) including the name “Chara”, but is hereafter referred to as Beta CVn. The star has been identified as a target of astrobiological significance due to both its similarity and proximity to the Sun (Porto de Mello et al. 2006; Turnbull 2015). Although no planets have been announced for the star, the limits on planetary companions based on survey data have yet to be demonstrated. Such limits on giant planets would potentially allow for greater dynamical diversity within the HZ, including scenarios of dynamically packed orbits that may otherwise be excluded due to secular resonances with giant planets in the system (Levison & Agnor 2003; Brassier et al. 2009; Kopparapu & Barnes 2010).

This paper explores the dynamical packing of terrestrial planets in the HZ as a function of spectral type. Section 2 uses stellar isochrones to quantify the width of the HZ as a function of stellar mass, describes the results of dynamical simulations of HZ packing of terrestrial planets, and demonstrates the effect of giant planets on HZ stability. In Section 3 we present the results of the Beta CVn case study, including stellar characterization, HZ region, and 20 years RV data from the Keck/HIRES and Automated Planet Finder (APF) facilities that rule out giant planets in the system. These data are used to estimate the potential for terrestrial planets in the HZ and prospects for direct imaging observations. We provide discussion of applications to future work and general conclusions in Section 4.

2. HABITABLE ZONE REAL ESTATE

2.1. Stellar Mass Dependence

The boundaries of the HZ have been cataloged for a variety of known exoplanetary systems (Kane & Gelino 2012), including the candidate exoplanet systems discovered by the *Kepler* mission (Kane et al. 2016; Hill et al. 2018). The stellar distance plays a key role in determining the stellar properties that influence the HZ boundaries, highlighting the importance of accurate distance estimates (Johns et al. 2018; Kane 2018). Here we calculate the width of the HZ as a function of the stellar mass, since mass is one of the more critical intrinsic stellar properties that determines the overall stellar evolution pathway.

To investigate the width of the HZ region as a function of stellar mass for main sequence stars, we utilize the MESA Isochrones & Stellar Tracks (MIST), described in detail by Choi et al. (2016) and Dotter (2016). We adopted a solar metallicity and used an age of 3 Gyrs in order to encompass isochrones for stars more massive than the Sun, including a mass range of 0.137–1.199 M_{\odot} . For each stellar mass, we used the isochrone luminosity and effective temperature to calculate the HZ boundaries as formulated by Kopparapu et al. (2013, 2014). We adopt both the “conservative” and “optimistic” HZ boundaries, described in detail by Kane et al. (2016).

The extracted isochrone stellar parameters of luminosity (solid line) and effective temperature (dashed line) along with our calculations of the HZ width (dot-dashed line) are represented in Figure 1. The values for all three have been normalized to solar values, which is why they intersect at a normalized quantity of unity for a solar mass star. We further calculated the Hill radius for an Earth-mass planet located in the middle of the HZ for each stellar mass. These Hill radii were also normalized, this time to the Hill radius of the Earth, and are

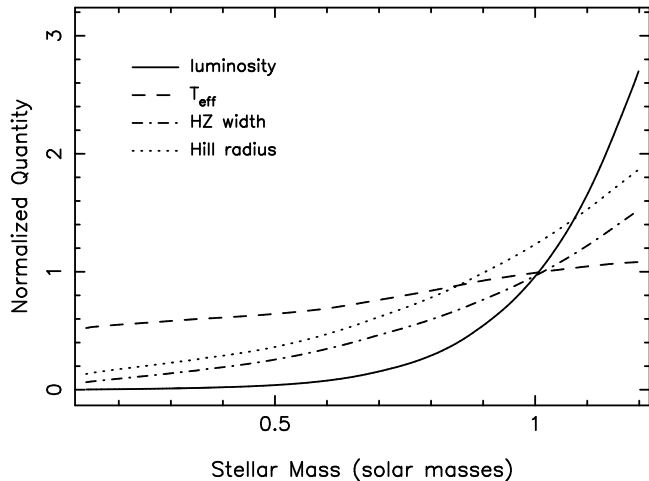


Figure 1. Stellar luminosity (solid line) and effective temperature (dashed line) as a function of stellar mass. For each of these values, we calculate the HZ width (dot-dashed line) and the Hill radius of an Earth-mass planet in the middle of the HZ (dotted line). For comparative purposes, the luminosity, effective temperature, and HZ have been normalized to solar values, and the Hill radius is normalized to the Earth value.

represented in Figure 1 as a dotted line. The rise in Hill radius with stellar mass is slightly less than the rise in HZ width. This implies that dynamical constraints on the number of planets in the HZ may increase with increasing stellar mass.

2.2. Dynamical Packing Limits

To test the dynamical limits of terrestrial planets within the HZ, we conducted an extensive suite of N-body integrations using the Mercury Integrator Package, described in detail by Chambers (1999). The simulations adopted the hybrid symplectic/Bulirsch-Stoer integrator with a Jacobi coordinate system, generally providing more accurate results for multi-planet systems (Wisdom & Holman 1991; Wisdom 2006). For each of the stellar masses extracted from the isochrones described in Section 2.1, we performed the following steps.

1. The boundaries of the optimistic HZ were calculated based on the stellar parameters.
2. Earth-mass planets were placed in circular orbits within the HZ, with one at the inner edge, one at the outer edge, and the others evenly spaced in between (Weiss et al. 2018). This was carried out for a range of 3–7 planets for each stellar mass.
3. The orbital period at the inner and outer edges of the HZ were calculated. The orbital period at the inner edge was used to determine the time step of the N-body integrations. These were set

to 1/20 of the inner edge orbital period to ensure perturbative reliability of the simulation, consistent with the recommendations of Duncan et al. (1998). The total simulation time was set to 10^8 times the orbital period at the outer edge of the HZ.

4. The dynamical simulation was carried out ~ 5 times with randomized starting locations (mean anomalies) for each of the planets to robustly capture the dynamical stability of the orbital architecture.
5. The assessment of stability was determined by requiring that all planets survive the duration of the simulation. Non-survival means that one or more of the planets has been captured by the gravitational well of the host star or ejected from the system.

Following the above steps resulted in several thousand simulations to fully explore the dynamical stability limits of packing evenly spaced terrestrial planets within the HZ for a range of stellar masses.

The results of the simulation suite described above are shown in Figure 2, where the colored shaded regions indicate the approximate spectral types that correspond to the stellar masses. For the 3 and 4 planet cases, we found that the dynamical integrity of the systems are retained for the entire range of stellar masses tested. We show the 5 planet case (solid line) as a demonstration of where instability begins to arise at the extreme low mass end of the stellar mass range. The 6 planet case (dashed line) exhibits significant instability within the HZ for stellar masses less than $\sim 0.7 M_{\odot}$. The trend of relative instability for lower mass stars is consistent with the relationship between the HZ width and the size of the Hill sphere discussed in Section 2.1. Significant collapse of the dynamical integrity for all stellar masses starts to occur for the 7 planet case (dotted line), with no stable scenarios for masses less than $\sim 0.25 M_{\odot}$. Furthermore, the stellar mass range of $0.8\text{--}1.1 M_{\odot}$ (G stars) is unlikely to harbor 7 evenly spaced planets within the HZ. Calculation of the corresponding orbital periods of the planets for this stellar mass range reveals a cause of mean motion resonances (MMRs). Specifically, the third planet in the sequence of 7 planets (from inner HZ edge to outer HZ edge) lies close to the 5:4 MMR with planet 4, the 3:2 MMR with planet 5, and 2:1 MMR with planet 7. These MMRs result in strong perturbative forces on planet 3 that are able to successfully compromise the system stability and rapidly lead to close encounters and subsequent ejections. Thus, in some cases, MMRs can lead to a potential additional advantage of K

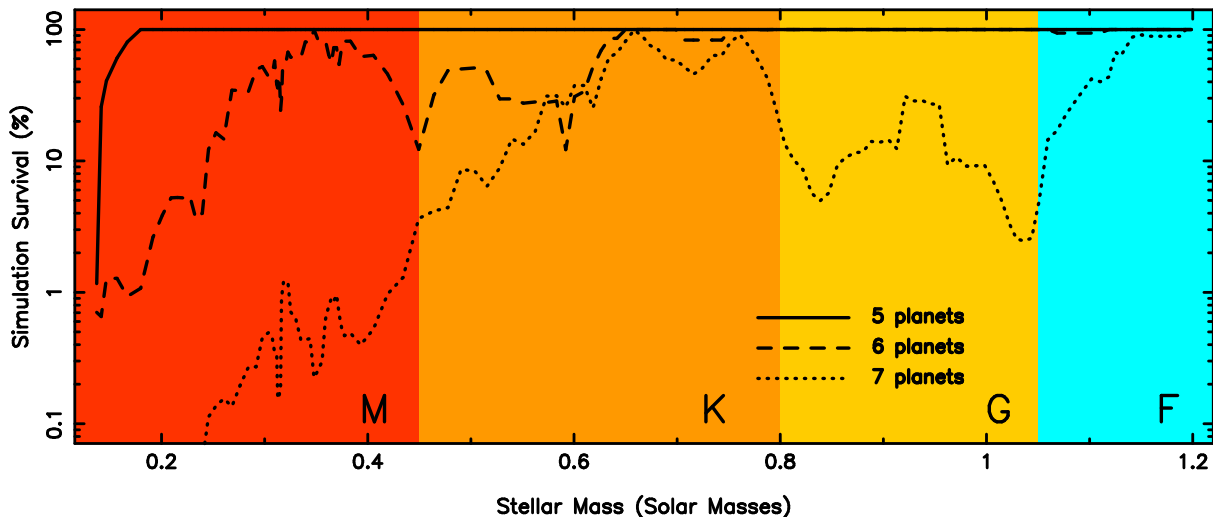


Figure 2. Simulation survival of the tested planetary architecture as a function of stellar mass, where the architecture consisted of evenly spaced Earth-mass planets for 3, 4, 5, 6, and 7 planets in the HZ, as described in Section 2.2. The cases of 5, 6, and 7 planets are shown as solid, dashed line, dotted lines respectively. The colored backgrounds indicate the corresponding spectral types (see bottom right of each colored region) for the stellar mass ranges shown.

dwarfs over G dwarfs for biosignature and direct imaging studies (Arney 2019).

For example, the case of our solar system has an optimistic HZ that extends from 0.74 AU to 1.73 AU. Our simulations show that 6 terrestrial planets are able to remain stable in this region but the 7 HZ planet architecture falls within the regime of MMR perturbations and catastrophic instability. This is consistent with the results of Smith & Lissauer (2009) and Obertas et al. (2017) whose simulations were for the specific solar mass case. These simulations neglect the effect of giant planets beyond the HZ that can also induce perturbative effects that can disrupt even the 6 planet scenarios.

2.3. Effects of Giant Planets

The number of known exoplanetary systems is now sufficient to develop statistical models that can predict orbital distributions based on collisional formation scenarios (Tremaine 2015). However, these distributions are greatly influenced by giant planets, particularly during their early periods of migration (Morbidelli & Raymond 2016). The presence of the giant planets in the solar system has undoubtedly played a significant role in the formation, evolution, and final architecture of the inner solar system (Tsiganis et al. 2005; Batygin & Laughlin 2015; Horner et al. 2020). Such important dynamical effects of giant planets have also shaped the architecture of other planetary systems (Matsumura et al. 2013; Morbidelli & Raymond 2016). Indeed, both the solar system and other planetary systems have been found to be close to instability boundaries that would compromise the dynamical in-

tegrity of those systems (Laskar 1996; Lecar et al. 2001; Murray & Holman 2001; Barnes & Quinn 2004). For example, a planet within the asteroid belt of the solar system would significantly alter the orbital dynamics of the inner solar system by exchanging angular momentum with the outer solar system (Lissauer et al. 2001).

With this in mind, the HZ packing scenarios described in Section 2.2 have been considered in isolation but are clearly dependent on the presence of other planets outside of the HZ, especially giant planets. Jupiter has a well-known perturbing influence at resonance locations, especially the induced chaos near the Kirkwood gaps (Wisdom 1983). The case of 7 planets within the HZ, described in Section 2.2, suffers from instability due to MMR effects internal to that region. External sources of MMR, particularly 5:2, 3:1, would result in similar sources of instability which would have a cascading transfer of angular momentum, similar to the asteroid belt planet scenario described by Lissauer et al. (2001). Therefore, the most likely cases of maximum terrestrial planets within the HZ are those solar-type stars for which giant planets may be excluded.

3. THE CASE OF BETA CVN

Here we consider the specific case for potential dynamical HZ packing of Beta CVn, a nearby solar analog (G0V).

3.1. Stellar Properties and Habitable Zone

The proximity, spectral type, and apparent brightness of Beta CVn have resulted in numerous observational studies of the star. The star has been found to be

photometrically and spectroscopically stable, resulting in its frequent use as an RV standard (Konacki 2005). A study of Sun-like stars by Radick et al. (2018) presented 18 years of Beta CVn photometry, acquired with the Automated Photoelectric Telescopes (Henry 1999). We extracted the Beta CVn photometry from their data collection and conducted a Fourier analysis of the complete time series. The highest peak in the power spectrum from this analysis occurs at 182.5 days, and is an observational artifact from the observing cadence. The second highest peak occurs at 110 days, which could be related to intrinsic stellar variability, although is too long for an expected rotation period.

Given the quiet nature of the star, the question arises as to the stellar equatorial plane relative to the plane of the sky since this will influence the detectability of planetary signatures, assuming those orbits are coplanar with the stellar equator. In order to optimize blind transit searches, Herrero et al. (2012) provided a catalog of stars whose inclination of the equatorial plane is likely $> 80^\circ$ relative to the plane of the sky. They adopt a rotational velocity of $v \sin i = 2.9 \text{ km s}^{-1}$ and activity index of $\log(R'_{HK}) = -4.885$ for Beta CVn, and their methodology predicts a high probability (50% larger than the average of their sample) of the star having an inclination $> 80^\circ$. The predicted probability is 10% higher than the mean probability for the host stars in their sample that are known to host transiting planets. This in turn increases the probability that any planets present are in close to edge-on orbits, increasing the expected RV signal.

The proximity of Beta CVn has also enabled several direct measurements of the stellar radius using interferometric techniques (van Belle & von Braun 2009; Boyajian et al. 2012). We adopt the stellar parameters provided by Boyajian et al. (2012), which include a stellar radius of $R_\star = 1.123 \pm 0.028 R_\odot$, a luminosity of $L_\star = 1.151 \pm 0.018 L_\odot$ and an effective temperature of $T_{\text{eff}} = 5653 \pm 72 \text{ K}$. Based on these stellar parameters, we calculate the conservative HZ as 1.03–1.82 AU and the optimistic HZ as 0.81–1.92 AU. The significance of the HZ distances for the star are described in more detail in Section 3.3.

3.2. No Giant Planets

Even though giant planets are more common around solar analogs than later-type stars (Zechmeister et al. 2013; Wittenmyer et al. 2016), they are still relatively rare, with an average occurrence rate of 6.7% beyond orbital periods of 300 days (Wittenmyer et al. 2020). Consequently, the solar system may not be representative of orbital architectures, and it is useful to directly com-

Table 1. Beta CVn Radial Velocities

Instrument	Date (BJD – 2450000)	RV (m s^{-1})	σ (m s^{-1})
HIRES _k	1551.1784	0.339	2.329
HIRES _k	1583.9661	-5.363	1.669
HIRES _k	1585.0081	-3.517	1.596
HIRES _k	1678.9005	-7.658	2.871
HIRES _k	1982.0561	-5.728	1.830
HIRES _k	2030.8898	-11.587	1.739
HIRES _k	2308.1046	-11.281	1.792
HIRES _k	2391.0513	-8.550	1.926
HIRES _k	2681.0914	-14.265	1.789
HIRES _k	2805.8423	-4.116	1.879
HIRES _k	3044.1802	-10.360	1.780
HIRES _k	3046.1807	-13.416	1.988
HIRES _j	3399.0412	4.337	1.230
HIRES _j	3399.0418	-1.512	1.197
HIRES _j	3399.0424	-4.692	1.123
HIRES _j	3480.7773	-1.325	1.089
HIRES _j	3480.7779	0.645	1.100
HIRES _j	3480.7785	-1.011	1.127
HIRES _j	3551.8156	-0.572	1.022
HIRES _j	3551.8162	-0.750	0.918
HIRES _j	3551.8168	-0.070	0.946
HIRES _j	3551.8174	0.737	1.005
HIRES _j	3725.1611	-2.464	1.253
HIRES _j	3725.1617	-0.609	1.169
HIRES _j	3747.1081	0.014	1.121

The full data set is available online.

pare with another nearby solar-type star, such as Beta CVn. To determine the limits on such giant companions, we present here 235 precision RV measurements of Beta CVn acquired over a period of 20 years. Observations were carried out using the HIRES echelle spectrograph on the Keck I telescope (Vogt et al. 1994) and the Levy spectrometer on the Automated Planet Finder (APF) (Radovan et al. 2014; Vogt et al. 2014). A subset of the RV data are shown in Table 1, where all the data have been calibrated to the same zero-point. Table 1 also includes a column for the instrument that was used to acquire the data. Note that the HIRES subscripts refer to data that were acquired prior to the 2004 upgrade to the instrument (k) and those that were acquired after (j). The data from all three instruments are shown plotted in Figure 3.

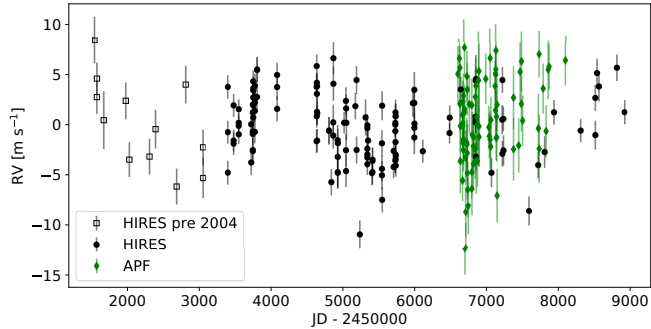


Figure 3. The RV data for Beta CVn plotted against observation time, including data from HIRES pre-2004 upgrade (HIRES_k), HIRES post-2004 upgrade (HIRES_j), and APF.

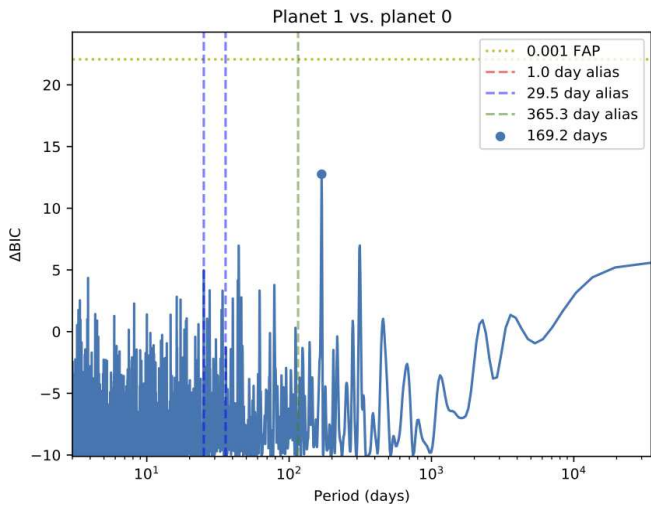


Figure 4. Power spectrum from a Fourier analysis of the RV data shown in Figure 3. Significant observational alias locations (diurnal, lunar, annual) are shown as vertical dashed lines. The highest peak occurs at a period of 169.2 days.

We performed a Fourier analysis of the RV data to investigate possible periodic signals. The periodogram resulting from this analysis is shown in Figure 4. The horizontal dotted line indicates a false-alarm probability (FAP) threshold of 0.001 (0.1%). The vertical dashed lines show the location of common aliases caused by the Earth’s rotation (diurnal) and orbital (annual) motions, as well as that caused by the lunar orbit. The highest peak occurs at a period of 169.2 days, which is still well below the FAP threshold. We conclude that there are no significant periodic signals present in the data.

The RV data described here were used to perform an injection-recovery test to quantify the completeness of the observations for excluding planetary signatures. This method injects planetary signatures of various masses ($M_p \sin i$) and semi-major axes (a) into the data using the same observation epochs and noise properties of the data. Circular orbits are assumed and the Kepler-

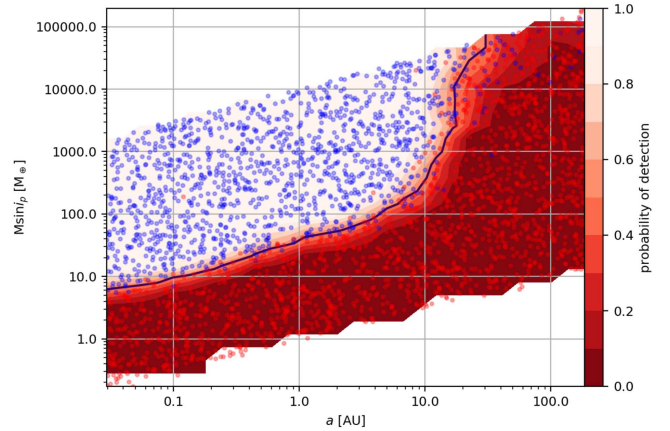


Figure 5. Results of the injection-recovery test to determine the sensitivity of the RV data to planetary signatures as a function of planetary mass ($M_p \sin i$) and semi-major axis (a). The blue dots represent injected planetary signatures that were successfully recovered and the red dots represent those planets that were not recovered. The color scale corresponding to the probability contours of detecting a planet of a given mass and semi-major axis is shown on the right vertical axis.

rian orbital fits are performed using the RadVel package (Fulton et al. 2018). The methodology for this process, including the criteria for planetary signature recovery, is described in detail by Howard & Fulton (2016). To perform the injection-recovery test in terms of $M_p \sin i$, a stellar mass must be assumed. There are a variety of estimates for the mass of Beta CVn in the literature, including $1.05 \pm 0.14 M_\odot$ by Valenti & Fischer (2005) and $0.852 \pm 0.023 M_\odot$ by Boyajian et al. (2012). We adopt the latter of these to be consistent with the stellar parameters used to calculate the HZ in Section 3.1.

The results of the injection-recovery test are shown in Figure 5. The blue dots represent injected planets that were recovered and the red dots represent those that were not recovered. The shaded contours indicate the probability of a successful detection, with the color scale shown on the right vertical axis. The results thus demonstrate that the RV data are sufficient to rule out the presence of $100 M_\oplus$ planets out to ~ 5 AU and $300 M_\oplus$ (Jupiter mass) planets out to ~ 10 AU. These data are thus sufficient to rule out the presence of most giant planets around Beta CVn inside an orbital radius of 10 AU. Note however that the data are not sufficient to rule out terrestrial planets in the system.

3.3. Potential for Terrestrial Planets

As described in Sections 2.2 and 2.3, the relative lack of giant planets in the Beta CVn system may allow for the presence of numerous terrestrial planets in a HZ dynamical packing scenario. Based on Figure 2 and the

Table 2. HZ Exoplanet Signatures

Parameter	Inner HZ	Outer HZ
P (days)	288.4	1052.6
K (m s^{-1})	0.108	0.070
d (%)	0.007	0.007
p (%)	0.65	0.27

stellar mass adopted in Section 3.2, the HZ of the star would be unlikely to contain 7 terrestrial planets even without a giant planet due to internal MMR perturbation effects. Beta CVn may therefore be a suitable system for which to test HZ packing scenarios.

As calculated in Section 3.1, the optimistic HZ of the system extends from 0.81 AU to 1.92 AU. Continuing to use the stellar parameters of Boyajian et al. (2012), we calculate several predicted exoplanet signatures at the inner and outer edge of the optimistic HZ, shown in Table 2. These include the orbital period P , the RV semi-amplitude K , the transit depth d , and the transit probability p (Kane & von Braun 2008). As expected, the K values are well below that required of the RV data presented in this work, but may be feasible with developing facilities (Fischer et al. 2016). Additionally, the work of Herrero et al. (2012) showed that Beta CVn has a relatively high probability that the inclination of the equatorial plane is $> 80^\circ$ relative to the plane of the sky (see Section 3.1), and so the transit probabilities are likely underestimated.

However, a further option to explore the possible planetary architecture of Beta CVn, particularly given the proximity of the star, is direct imaging (Kane et al. 2018; Dulz et al. 2020). At a stellar distance of 8.44 pcs, the 0.81–1.92 AU optimistic HZ translates into angular separations of 96–227 mas. Consistent with the final reports of the Habitable Exoplanet Observatory (HabEx) mission (Gaudi et al. 2020) and the Large UV/Optical/Infrared Surveyor (LUVOIR) mission (The LUVOIR Team 2019), we assume (a) an inner working angle (IWA) of ~ 58 mas, and (b) a contrast limit of $\sim 4 \times 10^{-11}$, which corresponds to the Earth–Sun contrast ratio at the outer edge of the Sun’s conservative HZ (1.7 AU).

Given the above assumptions, Figure 6 shows the stars having the largest fraction of their HZs falling within the detection limits of the instrument (scaled by the Hill radius), and the maximum V-band brightness of Earth analogs within the detectable HZ space, assuming a Bond albedo of 0.3. The color of the stars shown in the figure represents the effective temperature (spectral

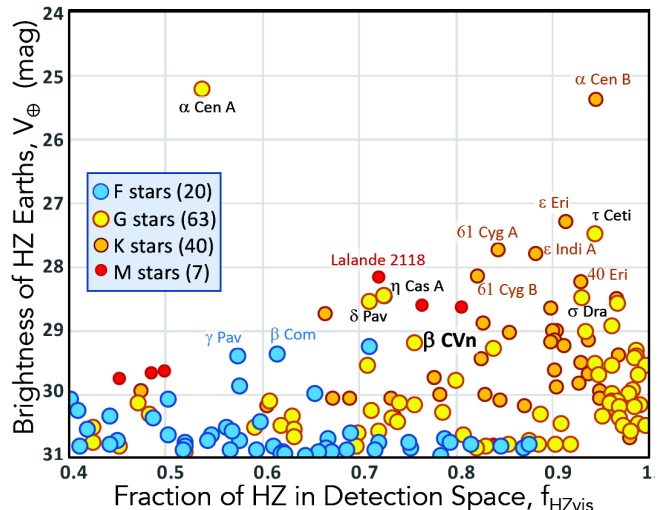


Figure 6. Calculated V-band magnitude of an Earth analog in the HZ of the nearest stars, as a function of the fraction of the HZ for those stars that are within instrument detection limits, scaled by the Hill radius. The color of the stars indicates their effective temperature (spectral type) and labels are provided for well-known nearby stars, including Beta CVn.

type) of the host stars, with M red, K orange, G yellow, and F cyan; similar to Figure 2. The most promising targets are shown in the right of the plot where both the predicted HZ Earth analog brightness and the visibility of the HZ are largest. For example, Beta CVn has a fractional HZ visibility of $\sim 75\%$ and an expected Earth analog brightness of $V \sim 29$. Note that the stellar sample shown in Figure 6 is dominated by K and G dwarfs for which the occupancy of the HZ by such Earth analogs is maximized, except in cases where internal MMRs truncate the number of allowed orbits (see Figure 2). Thus, direct imaging with facilities that meet the criteria laid down in the HabEx and LUVOIR reports may naturally favor targets that are predisposed towards larger than expected HZ planet inventories.

4. CONCLUSIONS

The search for potentially habitable exoplanets has an intrinsic relationship to their occurrence rates, a factor that has rapidly emerged in recent years. These occurrence rates are mostly being informed by transit surveys that are biased toward HZ planets around low-mass stars and have revealed a plethora of compact system architectures. Some of these systems, such as TRAPPIST-1, have been found to have multiple terrestrial planets in the HZ, causing speculation as to whether such dynamical packing in the HZ is normal or rare. Our analysis presented here demonstrates that in fact the dynamical limitations to the packing of HZ terrestrial planets is ~ 5 planets for most spectral types, and ~ 6 planets

for stellar masses $\gtrsim 0.7M_{\odot}$. Packing 7 planets in the HZ is possible within certain specific stellar mass and architecture regimes, but becomes vulnerable to MMR perturbations that compromise the dynamical stability of such configurations. The 20 years of RV data for Beta CVn presented here rule out a large range of giant planet masses and orbital parameters, providing an excellent candidate for complex terrestrial architectures.

There are some caveats to the analysis presented here that are worth repeating. First, Section 2.1 describes the use of 3 Gyr isochrones, which are adopted in order to include stars at the higher mass end of the stellar mass range. However, the star will evolve with time, as will the HZ (Gallet et al. 2017), resulting in an increase in both the width and orbital distance of the HZ. Subsequently, planets located at the inner edge of the HZ at 3 Gyr will transition into the Venus Zone (Kane et al. 2014) where runaway greenhouse scenarios may become dominant. Second, our simulations account for Earth-mass planets and circular orbits. Higher masses and non-zero eccentricities will reduce orbital stability within the HZ, but lower mass planets may allow for additional planets, with the exception of strong resonance regions.

The formation and final architecture of planetary systems depend on disk mass and migration scenarios (Raymond et al. 2005; Morbidelli & Raymond 2016; Dempsey et al. 2020). Indeed, formation simulations have demonstrated that terrestrial planets in the HZ are more likely to occur in the absence of giant planets beyond the snow line (Raymond et al. 2012; de Elía et al. 2013). Thus, the presence of multiple terrestrial planets in the HZ of a particular system depends on numerous factors related to the specific disk properties and formation processes. However, it should be noted that dynamical packing of terrestrial planets can have implications for, and even remove, other planetary and system properties that may be important for habitability. For example, although compact systems can clearly exist within the HZ, their potential for harboring moons are considerably truncated by the reduced Hill radii (Kane 2017). Similarly, dynamically packed systems around solar-type stars may experience long-term perturbations that limit the presence of moons for such planets. It is therefore worth considering in detail how HZ dynamical packing influences overall planetary evolution.

If such dynamical packing scenarios do exist in relative abundance, one could speculate as to why such systems have yet to be discovered. The difficulty with transit

detection is imposed by both the transit probability, the required duration of the survey, and the assumption of coplanarity with the HZ regime. Likewise, Table 2 highlights the challenges of RV detection given the relatively small expected semi-amplitude of the planetary signatures. In the coming years, the next generation of precision RV instruments may be able to address this challenge. Current RV surveys can rule out the presence of giant planets in nearby systems (e.g., Fischer et al. 2016, and references therein), thus providing potential targets that maximize the likelihood for dynamical packing. Further into the NASA mission timeline, space-based direct imaging missions, such as LUVOIR and HabEx, may acquire family portraits that finally reveal the true HZ architecture of planetary systems without giant planets.

ACKNOWLEDGEMENTS

The authors would like to thank Paul Dalba, Joshua Pepper, and the anonymous referee for their constructive feedback on the manuscript. We also thank Debra Fischer, John Johnson, Kathryn Peek, and Jason Wright for their contributions to the Keck observations. We gratefully acknowledge the efforts and dedication of the Keck Observatory staff for support of HIRES and remote observing. We recognize and acknowledge the cultural role and reverence that the summit of Maunakea has within the indigenous Hawaiian community. We are deeply grateful to have the opportunity to conduct observations from this mountain. We thank Ken and Gloria Levy, who supported the construction of the Levy Spectrometer on the Automated Planet Finder. We thank the University of California and Google for supporting Lick Observatory and the UCO staff for their dedicated work scheduling and operating the telescopes of Lick Observatory. This research has made use of the following archives: the Habitable Zone Gallery at hz-gallery.org and the NASA Exoplanet Archive, which is operated by the California Institute of Technology, under contract with the National Aeronautics and Space Administration under the Exoplanet Exploration Program. The results reported herein benefited from collaborations and/or information exchange within NASA's Nexus for Exoplanet System Science (NExSS) research coordination network sponsored by NASA's Science Mission Directorate.

Software: Mercury (Chambers 1999), RadVel (Fulton et al. 2018)

REFERENCES

- Agnew, M. T., Maddison, S. T., Horner, J., & Kane, S. R. 2019, MNRAS, 485, 4703
- Akeson, R. L., Chen, X., Ciardi, D., et al. 2013, PASP, 125, 989

- Anglada-Escudé, G., Tuomi, M., Gerlach, E., et al. 2013, *A&A*, 556, A126
- Arney, G. N. 2019, *ApJL*, 873, L7
- Barnes, R., & Quinn, T. 2004, *ApJ*, 611, 494
- Batygin, K., & Laughlin, G. 2015, *Proceedings of the National Academy of Science*, 112, 4214
- Becker, J. C., & Adams, F. C. 2017, *MNRAS*, 468, 549
- Bonfils, X., Delfosse, X., Udry, S., et al. 2013, *A&A*, 549, A109
- Boyajian, T. S., McAlister, H. A., van Belle, G., et al. 2012, *ApJ*, 746, 101
- Brasser, R., Morbidelli, A., Gomes, R., Tsiganis, K., & Levison, H. F. 2009, *A&A*, 507, 1053
- Catanzarite, J., & Shao, M. 2011, *PASP*, 123, 171
- Chambers, J. E. 1999, *MNRAS*, 304, 793
- Choi, J., Dotter, A., Conroy, C., et al. 2016, *ApJ*, 823, 102
- Cumming, A., Butler, R. P., Marcy, G. W., et al. 2008, *PASP*, 120, 531
- de Elía, G. C., Guilera, O. M., & Brunini, A. 2013, *A&A*, 557, A42
- Dempsey, A. M., Lee, W.-K., & Lithwick, Y. 2020, *ApJ*, 891, 108
- Dotter, A. 2016, *ApJS*, 222, 8
- Dressing, C. D., & Charbonneau, D. 2013, *ApJ*, 767, 95
- . 2015, *ApJ*, 807, 45
- Dulz, S. D., Plavchan, P., Crepp, J. R., et al. 2020, *ApJ*, 893, 122
- Duncan, M. J., Levison, H. F., & Lee, M. H. 1998, *AJ*, 116, 2067
- Endl, M., Cochran, W. D., Kürster, M., et al. 2006, *ApJ*, 649, 436
- Fang, J., & Margot, J.-L. 2013, *ApJ*, 767, 115
- Fischer, D. A., Anglada-Escudé, G., Arriagada, P., et al. 2016, *PASP*, 128, 066001
- Ford, E. B. 2014, *Proceedings of the National Academy of Science*, 111, 12616
- Foreman-Mackey, D., Hogg, D. W., & Morton, T. D. 2014, *ApJ*, 795, 64
- Fulton, B. J., Petigura, E. A., Blunt, S., & Sinukoff, E. 2018, *PASP*, 130, 044504
- Gaidos, E. 2013, *ApJ*, 770, 90
- Gallet, F., Charbonnel, C., Amard, L., et al. 2017, *A&A*, 597, A14
- Gaudi, B. S., Seager, S., Mennesson, B., et al. 2020, *arXiv e-prints*, arXiv:2001.06683
- Gillon, M., Triaud, A. H. M. J., Demory, B.-O., et al. 2017, *Nature*, 542, 456
- Henry, G. W. 1999, *PASP*, 111, 845
- Herrero, E., Ribas, I., Jordi, C., Guinan, E. F., & Engle, S. G. 2012, *A&A*, 537, A147
- Hill, M. L., Kane, S. R., Seperuelo Duarte, E., et al. 2018, *ApJ*, 860, 67
- Horner, J., & Jones, B. W. 2008, *International Journal of Astrobiology*, 7, 251
- Horner, J., Vervoort, P., Kane, S. R., et al. 2020, *AJ*, 159, 10
- Howard, A. W., & Fulton, B. J. 2016, *PASP*, 128, 114401
- Johns, D., Marti, C., Huff, M., et al. 2018, *ApJS*, 239, 14
- Johnson, J. A., Aller, K. M., Howard, A. W., & Crepp, J. R. 2010, *PASP*, 122, 905
- Kane, S. R. 2015, *ApJL*, 814, L9
- . 2017, *ApJL*, 839, L19
- . 2018, *ApJL*, 861, L21
- Kane, S. R., & Blunt, S. 2019, *AJ*, 158, 209
- Kane, S. R., & Gelino, D. M. 2012, *PASP*, 124, 323
- Kane, S. R., Hinkel, N. R., & Raymond, S. N. 2013, *AJ*, 146, 122
- Kane, S. R., Kopparapu, R. K., & Domagal-Goldman, S. D. 2014, *ApJL*, 794, L5
- Kane, S. R., Meshkat, T., & Turnbull, M. C. 2018, *AJ*, 156, 267
- Kane, S. R., & von Braun, K. 2008, *ApJ*, 689, 492
- Kane, S. R., Hill, M. L., Kasting, J. F., et al. 2016, *ApJ*, 830, 1
- Kasting, J. F., Whitmire, D. P., & Reynolds, R. T. 1993, *Icarus*, 101, 108
- Konacki, M. 2005, *ApJ*, 626, 431
- Kopparapu, R. K. 2013, *ApJ*, 767, L8
- Kopparapu, R. K., & Barnes, R. 2010, *ApJ*, 716, 1336
- Kopparapu, R. K., Ramirez, R. M., SchottelKotte, J., et al. 2014, *ApJ*, 787, L29
- Kopparapu, R. K., Raymond, S. N., & Barnes, R. 2009, *ApJ*, 695, L181
- Kopparapu, R. K., Ramirez, R., Kasting, J. F., et al. 2013, *ApJ*, 765, 131
- Laskar, J. 1996, *Celestial Mechanics and Dynamical Astronomy*, 64, 115
- Lecar, M., Franklin, F. A., Holman, M. J., & Murray, N. J. 2001, *ARA&A*, 39, 581
- Levison, H. F., & Agnor, C. 2003, *AJ*, 125, 2692
- Lissauer, J. J., Quintana, E. V., Rivera, E. J., & Duncan, M. J. 2001, *Icarus*, 154, 449
- Luger, R., Sestovic, M., Kruse, E., et al. 2017, *Nature Astronomy*, 1, 0129
- Matsumura, S., Ida, S., & Nagasawa, M. 2013, *ApJ*, 767, 129
- Morbidelli, A., & Raymond, S. N. 2016, *Journal of Geophysical Research (Planets)*, 121, 1962
- Murray, N., & Holman, M. 2001, *Nature*, 410, 773

- Obertas, A., Van Laerhoven, C., & Tamayo, D. 2017, *Icarus*, 293, 52
- Porto de Mello, G., del Peloso, E. F., & Ghezzi, L. 2006, *Astrobiology*, 6, 308
- Pu, B., & Wu, Y. 2015, *ApJ*, 807, 44
- Radick, R. R., Lockwood, G. W., Henry, G. W., Hall, J. C., & Pevtsov, A. A. 2018, *ApJ*, 855, 75
- Radovan, M. V., Lanclos, K., Holden, B. P., et al. 2014, *Society of Photo-Optical Instrumentation Engineers (SPIE) Conference Series*, Vol. 9145, The automated planet finder at Lick Observatory (SPIE Press), 91452B
- Raymond, S. N., Quinn, T., & Lunine, J. I. 2005, *ApJ*, 632, 670
- Raymond, S. N., Armitage, P. J., Moro-Martín, A., et al. 2012, *A&A*, 541, A11
- Shields, A. L., Ballard, S., & Johnson, J. A. 2016, *PhR*, 663, 1
- Smith, A. W., & Lissauer, J. J. 2009, *Icarus*, 201, 381
- . 2010, *Celestial Mechanics and Dynamical Astronomy*, 107, 487
- The LUVOIR Team. 2019, arXiv e-prints, arXiv:1912.06219
- Tremaine, S. 2015, *ApJ*, 807, 157
- Tsiganis, K., Gomes, R., Morbidelli, A., & Levison, H. F. 2005, *Nature*, 435, 459
- Turnbull, M. C. 2015, arXiv e-prints, arXiv:1510.01731
- Valenti, J. A., & Fischer, D. A. 2005, *ApJS*, 159, 141
- van Belle, G. T., & von Braun, K. 2009, *ApJ*, 694, 1085
- Vogt, S. S., Allen, S. L., Bigelow, B. C., et al. 1994, *Society of Photo-Optical Instrumentation Engineers (SPIE) Conference Series*, Vol. 2198, HIRES: the high-resolution echelle spectrometer on the Keck 10-m Telescope (SPIE Press), 362
- Vogt, S. S., Radovan, M., Kibrick, R., et al. 2014, *PASP*, 126, 359
- Weiss, L. M., Marcy, G. W., Petigura, E. A., et al. 2018, *AJ*, 155, 48
- Wisdom, J. 1983, *Icarus*, 56, 51
- . 2006, *AJ*, 131, 2294
- Wisdom, J., & Holman, M. 1991, *AJ*, 102, 1528
- Wittenmyer, R. A., Butler, R. P., Tinney, C. G., et al. 2016, *ApJ*, 819, 28
- Wittenmyer, R. A., Butler, R. P., Horner, J., et al. 2020, *MNRAS*, 491, 5248
- Zechmeister, M., Kürster, M., Endl, M., et al. 2013, *A&A*, 552, A78
- Zechmeister, M., Dreizler, S., Ribas, I., et al. 2019, *A&A*, 627, A49